arXiv:1408.6072v3 [cond-mat.mes-hall] 21 Apr 2015

Chimeras in SQUID Metamaterials

N. Lazarides[1,2], G. Neofotistos[1], G. P. Tsironis[1,2,3]
[1] *Crete Center for Quantum Complexity and Nanotechnology, Department of Physics, University of Crete, P. O. Box 2208, 71003 Heraklion, Greece;*
[2] *Institute of Electronic Structure and Laser, Foundation for Research and Technology-Hellas, P.O. Box 1527, 71110 Heraklion, Greece;*
[3] *Department of Physics, School of Science and Technology, Nazarbayev University, 53 Kabanbay Batyr Ave., Astana 010000, Kazakhstan*
(Dated: April 22, 2015)

Regular lattices comprising Superconducting QUantum Interference Devices (SQUIDs) form magnetic metamaterials exhibiting extraordinary properties, including tuneability, dynamic multistability, and negative magnetic permeability. The SQUIDs in a metamaterial interact through non-local, magnetic dipole-dipole forces, that makes it possible for counter-intuitive dynamic states referred to as *chimera states* to appear; the latter feature clusters of SQUIDs with synchronous dynamics which coexist with clusters exhibiting asynchronous behavior. The spontaneous appearence of *chimera states* is demonstrated numerically for one-dimensional SQUID metamaterials driven by an alternating magnetic field in which the fluxes threading the SQUID rings are randomly initialized; then, chimera states appear generically for sufficiently strong initial excitations, which exhibit relatively long life-times. The synchronization and metastability levels of the chimera states are discussed in terms of appropriate measures. Given that both one- and two-dimensional SQUID metamaterials have been already fabricated and investigated in the lab, the presence of a chimera state could in principle be detected with presently available experimental set-ups.

PACS numbers: 05.65.+b,05.45.Xt,78.67.Pt,89.75.-k,89.75.Kd

I. INTRODUCTION

Superconducting QUantum Interference Device (SQUID) metamaterials constitute a subclass of superconducting artificial media whose function relies both on the geometry and the extraordinary properties of superconductivity and the Josephson effect[1,2]. Recent experiments on both one- and two-dimensional radio-frequency (rf) SQUID metamaterials in the superconducting state have demonstrated their wide-band tuneability, significantly reduced losses, and dynamic multistability[2–6]. The simpest version of an rf SQUID consists of a superconducting ring interrupted by a Josephson junction[7] (Fig. 1a); that device is a highly nonlinear resonator with a strong response to applied magnetic fields. SQUID metamaterials exhibit peculiar magnetic properties including negative diamagnetic permeability that were predicted both for the quantum[8] and the classical[9] regime. The applied alternating fields induce (super)currents in the SQUID rings, coupling them together through dipole-dipole magnetic forces; although weak due to its magnetic nature, that interaction couples the SQUIDs non-locally since it falls-off as the inverse cube of their center-to-center distance.

The study of networks of interacting nonlinear elements pervades all of science, from neurobiology to statistical physics, often revealing remarkable aspects of collective behaviour[10]. The effect of non-local interactions, which constitutes the "dark corner" of nonlinear dynamics, has been extensively investigated in the last decade and has unveiled collective dynamic effects such as synchronization[11,12], pattern formation[13], and Turing instabilities[14]. Recently, a state with a counter-intuitive structure, usually referred to as a *"chimera state"*, was discovered in numerical simulations of non-locally coupled oscillator arrays[15]. Since then, an intense theoretical[16–29] and experimental[30–40] activity has been initiated. A *"chimera state"* is characterized by the coexistence of synchronous and asynchronous clusters (subgroups) of oscillators, even though they are coupled symmetrically and they are identical[41,42]. In the present work, it is demonstrated numerically that this remarkable collective dynamic behaviour emerges in SQUID metamaterials which are driven by an alternating magnetic field in the presence of weak dissipation. The SQUID metamaterial model which has been used previously in the weak and local coupling regime, in which each SQUID is only coupled to its nearest neighbors, for the investigation of intrinsic localization and tuneability effects[43–45], is being extended to account for non-local magnetic interactions.

Chimera states with very long life-times are obtained by initializing randomly the fluxes threading the SQUID rings; the subsequent dynamic evolution yields spontaneous formation of clusters of SQUIDs that exhibit synchronous and asynchronous flux oscillations for sufficiently strong initial flux excitations. Their existence requires multistability of the individual SQUIDs at frequencies in the region around that of the driving field. Individual SQUID states with high current amplitude may customarily be reached from basins of attraction which are much smaller than those of the states with low current amplitude. The number of possible states in a SQUID metamaterial is not merely the sum of the combinations of individual SQUID states, since their collective behavior may provide many more possibilities. Chimera

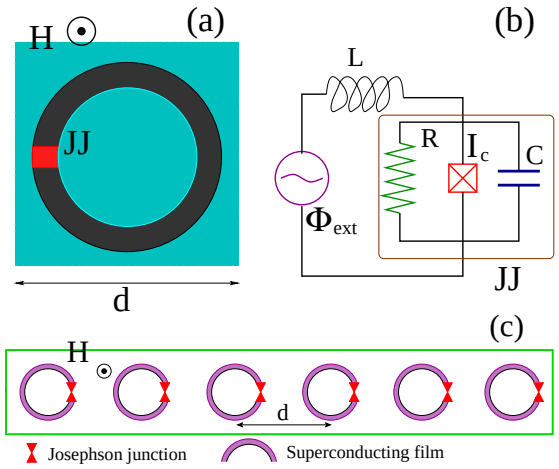

FIG. 1: (Color online) Schematic of an rf SQUID in an alternating magnetic field $\mathbf{H}(t)$ (a), and equivalent electrical circuit (b). The real Josephson junction is represented by the circuit elements that are in the brown-dashed box. (c) A one-dimensional SQUID metamaterial is formed by repetition of the squared unit cell of side d shown in (a).

states are such an example, where qualitatively distinct and counter-intuitive states emerge from collective dynamics. Although chimera states are generally regarded to be metastable[46,47], or even chaotic transients[48], there are also examples where they are at the global minimum of a system in thermal equilibrium, as has been predicted for Ising spins[49]. The level of synchronization and metastability of the chimera states can be however quantified by several measures[46,47]. Many different types of non-local interactions have been employed in the literature, often exponentially decaying, that allow a particular system to reach a chimera state. Importantly, chimera states in globally coupled systems that have been recently demonstrated[29,50], may lead to a revision of their existence criteria. The magnetic dipole-dipole interaction between SQUIDs, considered here, although it is still short-ranged[51], it falls-off much slower than the exponentially decaying one and it is capable of rendering the system able to support chimera states.

In the next Section, the non-locally coupled SQUID metamaterial model is presented, and the linear frequency dispersion is obtained. In the same Section, the complex synchronization (Kuramoto-type) parameter is defined along with a measure of metastability. In Section III, the numerically obtained spatiotemporal evolution of several chimera states are shown, and compared with those of the corresponding locally coupled SQUID metamaterial. The magnitude of the synchronization parameter is monitored in time both for the non-locally and the locally coupled SQUID metamaterials, and the differences are indicated. The metastability of the chimera states is discussed in terms of the full-width half-maximum of the distribution of the magnitude of the synchronization parameter at each time-instant. The conclusions are given in the last Section.

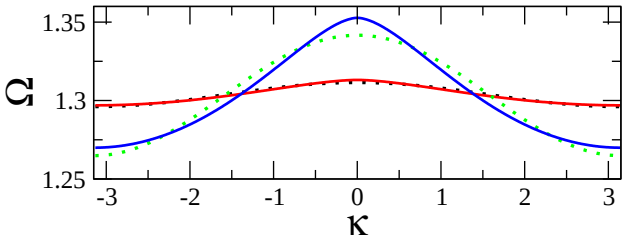

FIG. 2: (Color online) Frequency dispersion of the SQUID metamaterial with non-local coupling, for $\beta = 0.1114$ ($\beta_L \simeq 0.7$) and $\lambda_0 = -0.05$ (blue curve); -0.01 (red curve). The corresponding dispersions for nearest neighbor coupling are shown as green and black dotted curves, respectively.

II. SQUID METAMATERIAL MODELLING AND MEASURE OF SYNCHRONIZATION

Consider a one-dimensional linear array of N identical SQUIDs coupled together magnetically through dipole-dipole forces. The magnetic flux Φ_n threading the $n-$th SQUID loop is

$$\Phi_n = \Phi_{ext} + L\, I_n + L \sum_{m \neq n} \lambda_{|m-n|} I_m, \qquad (1)$$

where the indices n and m run from 1 to N, Φ_{ext} is the external flux in each SQUID, $\lambda_{|m-n|} = M_{|m-n|}/L$ is the dimensionless coupling coefficient between the SQUIDs at positions m and n, with $M_{|m-n|}$ being their corresponding mutual inductance, and

$$-I_n = C\frac{d^2\Phi_n}{dt^2} + \frac{1}{R}\frac{d\Phi_n}{dt} + I_c \sin\left(2\pi\frac{\Phi_n}{\Phi_0}\right) \qquad (2)$$

is the current in each SQUID given by the resistively and capacitively shunted junction (RCSJ) model[52], with Φ_0 and I_c being the flux quantum and the critical current of the Josephson junctions, respectively. Within the RCSJ framework, R, C, and L are the resistance, capacitance, and self-inductance of the SQUIDs' equivalent circuit (Fig. 1b). Combination of Eqs. (1) and (2) gives

$$C\frac{d^2\Phi_n}{dt^2} + \frac{1}{R}\frac{d\Phi_n}{dt} + \frac{1}{L}\sum_{m=1}^{N}\left(\hat{\mathbf{\Lambda}}^{-1}\right)_{nm}(\Phi_m - \Phi_{ext}) + I_c \sin\left(2\pi\frac{\Phi_n}{\Phi_0}\right) = 0, \qquad (3)$$

where $\hat{\mathbf{\Lambda}}^{-1}$ is the inverse of the $N \times N$ coupling matrix

$$\hat{\mathbf{\Lambda}} = \begin{cases} 1, & \text{if } m = n; \\ \lambda_{|m-n|} = \lambda_0\, |m-n|^{-3}, & \text{if } m \neq n, \end{cases} \qquad (4)$$

with λ_0 being the coupling coefficient betwen nearest neighboring SQUIDs. In normalized form Eq. (3) reads

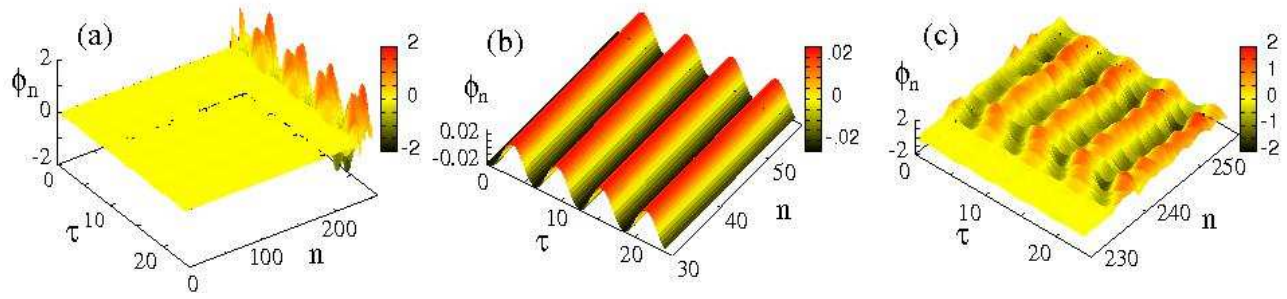

FIG. 3: (Color online) Spatio-temporal evolution of the normalized fluxes ϕ_n threading the SQUID rings during four driving periods $T = 5.9$ for $N = 256$, $\gamma = 0.0022$, $\lambda_0 = -0.05$, $\beta = 0.1114$ ($\beta_L \simeq 0.7$), $\phi_{ac} = 0.015$, and $\phi_R = 0.85$. (a) for the whole SQUID metamaterial; (b) for part of the metamaterial that belongs to the coherent cluster; (c) for part of the metamaterial that includes the incoherent cluster.

$(n = 1, ..., N)$

$$\ddot{\phi}_n + \gamma\dot{\phi}_n + \beta \sin(2\pi\phi_n) = \sum_{m=1}^{N} \left(\hat{\mathbf{\Lambda}}^{-1}\right)_{nm} (\phi_{ext} - \phi_m), \quad (5)$$

where the frequency and time are normalized to $\omega_0 = 1/\sqrt{LC}$ and its inverse ω_0^{-1}, respectively, the fluxes and currents are normalized to Φ_0 and I_c, respectively, the overdots denote derivation with respect to the normalized temporal variable, τ, $\phi_{ext} = \phi_{ac}\cos(\Omega\tau)$, with $\Omega = \omega/\omega_0$ being the normalized driving frequency, and

$$\beta = \frac{I_c L}{\Phi_0} = \frac{\beta_L}{2\pi}, \qquad \gamma = \frac{1}{R}\sqrt{\frac{L}{C}} \quad (6)$$

is the SQUID parameter and loss coefficient, respectively. The value of β_L determines whether a SQUID is hysteretic or non-hysteretic ($\beta_L > 1$ and $\beta_L < 1$, respectively).

Linearization of Eq. (5) around zero with $\gamma = 0$ and $\phi_{ext} = 0$ gives for the infinite system

$$\ddot{\phi}_n + \left[\beta_L + \left(\hat{\mathbf{\Lambda}}^{-1}\right)_{nn}\right]\phi_n + \sum_{m\neq n} \left(\hat{\mathbf{\Lambda}}^{-1}\right)_{nm} \phi_m = 0. \quad (7)$$

By substitution of $\phi_n = A\exp[i(\kappa n - \Omega\tau)]$ into Eq. (7), with κ being the wavevector normalized to d^{-1}, and using

$$\sum_{m\neq n} \left(\hat{\mathbf{\Lambda}}^{-1}\right)_{nm} e^{i\kappa(m-n)} = 2\sum_{m=1}^{\infty} \left(\hat{\mathbf{\Lambda}}^{-1}\right)_{m} \cos(\kappa m), \quad (8)$$

where m is the "distance" from the main diagonal of $\hat{\mathbf{\Lambda}}^{-1}$, we get

$$\Omega = \sqrt{\Omega_0^2 + 2\sum_{m=1}^{\infty} \left(\hat{\mathbf{\Lambda}}^{-1}\right)_{m} \cos(\kappa m)}, \quad (9)$$

where $\Omega_0^2 = \beta_L + \left(\hat{\mathbf{\Lambda}}^{-1}\right)_{nn} \simeq \beta_L + 1$. Note that for the infinite system the diagonal elements of the inverse of the coupling matrix $\left(\hat{\mathbf{\Lambda}}^{-1}\right)_{nn}$ have practically the same value which is slightly larger than unity. The frequency Ω_0 is very close to the resonance frequency of individual SQUIDs, $\Omega_{SQ} = \sqrt{\beta_L + 1}$. The nonlocal frequency dispersion Eq. (9) is slightly different from that obtained with only nearest-neighbor coupling (Fig. 2).

Eqs. (5) are numerically integrated in time using a fourth-order Runge-Kutta algorithm with fixed time stepping, typically $\Delta t = 0.02$, with $\phi_n(\tau = 0)$ randomly chosen from a flat, zero mean distribution in $[-\phi_R/2, +\phi_R/2]$ and $\dot{\phi}_n(\tau = 0) = 0$ for all n. The boundary conditions

$$\phi_0(\tau) = 0, \qquad \phi_{N+1}(\tau) = 0, \quad (10)$$

are used to account for the termination of the structrure in a finite system. The degree of synchronization for a given cluster of SQUIDs or for the whole SQUID metamaterial having M elements is quantified by introducing a complex, Kuramoto-type synchronization parameter $\Psi(\tau)$, defined as

$$\Psi(\tau) = \frac{1}{M}\sum_{m=1}^{M} e^{i[2\pi\phi_m(\tau)]}. \quad (11)$$

The magnitude of the synchronization parameter, $|\Psi(\tau)|$, provides a global (for the whole metamaterial) or local (within a cluster) measure of spatial coherence at time-instant τ. The value of $|\Psi(\tau)|$ lies in the interval $[0, 1]$, where the values 0 and 1 correspond to complete desynchronization and synchronization, respectively. The mean synchrony level $|\bar{\Psi}|$, which is an index of the global synchronization level, is defined as the average of $|\Psi(\tau)|$ over the time interval of integration[47], while the variance of $|\Psi(\tau)|$, $\sigma^2_{|\Psi|}$, captures how the degree of synchrony fluctuates in time. Fluctuations of the degree of synchronization have been associated with the existence of metastable states and therefore $\sigma^2_{|\Psi|}$ is indicative of the system's metastability level[46,47].

The parameters used in the simulations are rather typical for SQUID metamaterials. In Ref.[5], the values of

the SQUIDs' inductance, resistance, and capacitance are $L = 0.12\ nH$, $R = 840\ \Omega$, and $C = 0.65\ pF$, respectively, while the critical current is 3.7 μA and 1.2 μA at temperature $T = 4.2\ K$ and 6.5 K, respectively. Inserting these values in the first of Eqs. (6), we get for β_L the values 0.44 and 1.3 at $T = 4.2\ K$ and 6.5 K, respectively. Here we use $\beta_L = 0.7$, which lies in between those values, while our value of the amplitude of the alternating field $\phi_{ac} = 0.015$ lies within the range of values used in the experiments ($\phi_{ac} \simeq 0.006 - 0.05$). The coupling coefficient between nearest neighbors in Ref.[5] has been estimated to be $\lambda_0 \simeq -0.02$, using a simple approximation scheme in which the SQUIDs are regarded as thin rings. However, a large part of the area of the actual SQUID metamaterial is filled by superconducting material that the field cannot penetrate; it is thus expected that more magnetic flux than that predicted by the simple approximation will find its way through the SQUID rings, increasing thus considerably λ_0 (we use $\lambda_0 = -0.05$). The value of the loss coefficient in our simulations is $\gamma \simeq 0.002$, while from the second of Eqs. (6) and the values given in Ref.[5] we get ~ 0.02. Although the losses in the SQUIDs can be reduced considerably by lowering the temperature without affecting much the critical currents of the junctions, we have checked that chimera states also exist for γ of the order of ~ 0.02 when compensated by a larger ac field amplitude ϕ_{ac}.

Note that the comparison of the parameters used in the simulations of the one-dimensional SQUID metamaterial are compared with those in Ref.[5], in which the experiments have been performed on two-dimensional arrays, merely to show that these are realistic. In this work, we do not attempt to simulate a particular SQUID metamaterial. Moreover, the dimensionality of the system does not affect significantly the estimation of the parameters that are necessary for the simulations, since they can be estimated either by the individual SQUID properties (i.e., β, γ) or by a pair of SQUIDs (i.e., λ_0).

III. CHIMERA STATES: LEVELS OF SYNCHRONIZATION AND METASTABILITY

Chimera states are very sensitive to slight changes of the model parameters, the parameters of the driving field, as well as the integration parameters, e.g., the value of the time-step, and there is indeed a large number of such states available in a SQUID metamaterial. The chosen time-step $\Delta\tau = 0.02$, in particular, is a typical choice for systems of nonlinear oscillators that gives reliable results. Decreasing of the time-step (i.e., to $\Delta\tau = 0.01$) leads the SQUID metamaterial to a different chimera state due to their high metastability; that state may be either more or less synchronized than the previous one, depending on the other parameters. For the chosen parameters, the system reaches spontaneously dynamical states where synchronous (coherent) and asynchronous (incoherent) clusters of SQUIDs coexist, for most of the initial flux configurations with $\phi_R \sim \Phi_0$. A typical spatiotemporal flux pattern obtained after 10^7 time units (t.u.) of integration is shown in Fig. 3a, where the evolution of the ϕ_ns is monitored during four driving periods $T = 2\pi/\Omega$. Two different domains of the array can be distinguished, in which the fluxes through the SQUIDs are oscillating either with low or high amplitude. The enlargement of two particular subdomains shown in Figs. 3b and 3c reveals the main feature of a chimera state; besides the difference in the oscillation amplitudes (i.e., low-high), there are different dynamic behaviors: the low-amplitude oscillations are completely synchronized (Fig. 3b) while the high-amplitude ones are desynchronized both in phase and amplitude (Fig. 3c). Note that since the SQUID metamaterial is driven at a particular frequency Ω, there can be no net frequency drift as in phase oscillators[15]; instead, the period of each SQUID in the asynchronous cluster fluctuates around that of the driver, T.

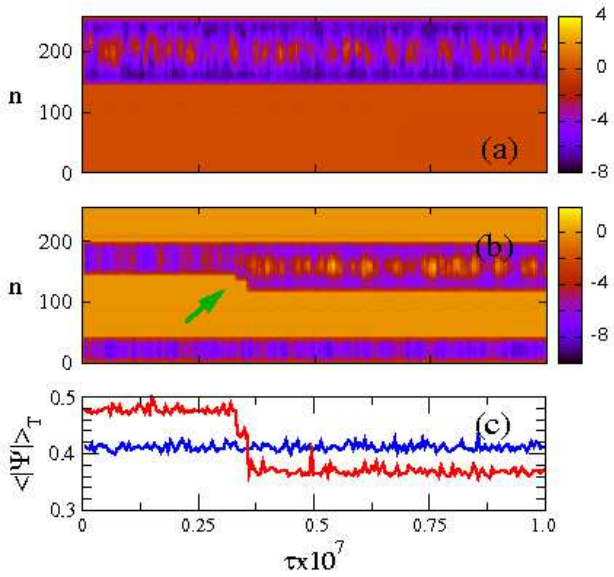

FIG. 4: (Color online) Density plot of the fluxes ϕ_n on the $n - \tau$ plane for a non-locally coupled SQUID metamatgerial with $T = 5.9$, $N = 256$, $\gamma = 0.0021$, $\lambda_0 = -0.05$, $\beta = 0.1114$ ($\beta_L \simeq 0.7$), $\phi_{ac} = 0.015$, and $\phi_R = 0.9$ (a); $\phi_R = 0.8$ (b). The green arrow indicates sudden expansions of the corresponding asynchronous cluster. (c) The corresponding magnitude of the Kuramoto parameter averaged over the driving period T, $< |\Psi(\tau)| >_T$ as a function of time τ; the blue and red curves are obtained for the chimera state shown in (a) and (b), respectively.

In Figs. 4a and 4b, the long-term spatiotemporal evolution for the fluxes ϕ_n is shown as a density plot on the $n - \tau$ plane for two different initial flux configurations; the values of the ϕ_ns are obtained at time-instants that are multiples of the driving period T, so that uniform (non-uniform) colorization indicates synchronous (asynchronous) dynamics. In Fig. 4a, two large clusters of SQUIDs have been apparently formed spontaneously, one with coherent and the other with incoherent dynamics.

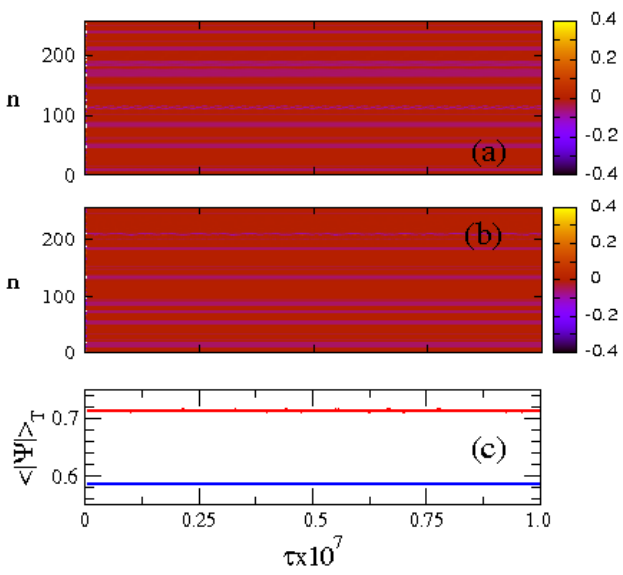

FIG. 5: (Color online) Density plot of the fluxes ϕ_n on the $n-\tau$ plane for a locally coupled SQUID metamaterial with $T = 5.9$, $N = 256$, $\gamma = 0.0021$, $\lambda_0 = -0.05$, $\beta_L = 0.7$ ($\beta \simeq 0.1114$), $\phi_{ac} = 0.015$, and $\phi_R = 0.9$ (a); $\phi_R = 0.8$ (b). (c) The corresponding magnitude of the Kuramoto parameter averaged over the driving period T, $< |\Psi(\tau)| >_T$ as a function of time τ; the blue and red curves are obtained for the non-uniform states shown in (a) and (b), respectively.

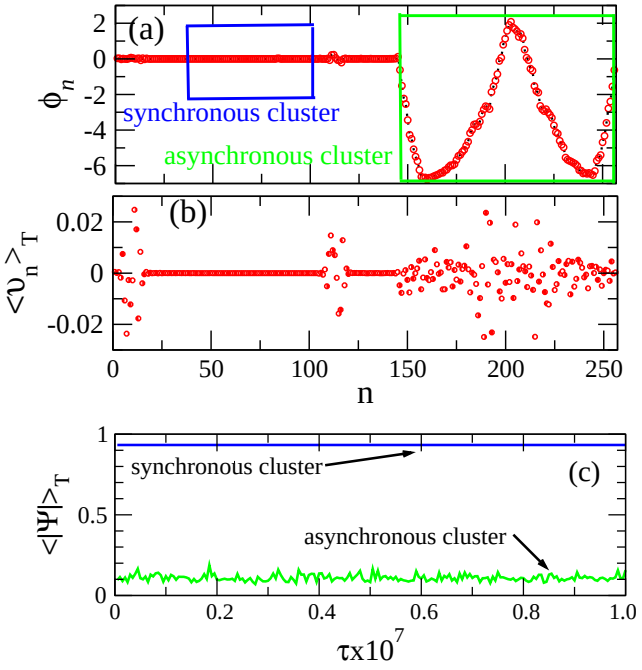

FIG. 6: (Color online) (a) Spatial profile of the fluxes ϕ_n threading the SQUID rings at $\tau = 10^7$ time units for the parameters of Fig. 4. (b) The corresponding averaged voltage profile $< v_n(\tau) >_T = < \dot{\phi}_n(\tau) >_T$. (c) The magnitude of the synchronization parameter averaged over T, $< |\Psi| >_T$, as a function of time τ, calculated for the coherent cluster in the small-blue box (blue curve) and for the incoherent cluster in the large-green box (green curve) in (a).

More SQUID clusters (two with synchronous and two with asynchronous behaviour) can be observed in Fig. 4b, in which the effect of metastability is reflected in the sudden expansions of the upper asynchronous cluster at around $\tau \sim 0.35 \times 10^7$ t.u. (green arrow). In the corresponding time-dependent magnitudes of the synchronization parameter averaged over the driving period T, $< |\Psi(\tau)| >_T$, those sudden expansions make themselves apparent as abrupt changes towards lower synchronization levels (Fig. 4c). By changing the coupling between the SQUIDs from non-local to local, i.e., by taking into account the coupling of each SQUID only to its nearest-neighbours, we obtain the corresponding patterns and $< |\Psi(\tau)| >_T$s shown in Fig. 5. The differences in the patterns of Figs. 4 and 5 are merely due to the change of the coupling from non-local to local. As can be observed in Figs. 5a and 5b, the SQUID metamaterial states are not uniform since a number of clusters have been formed; however, the dynamics within all these clusters is synchronous. The different states occupied by the SQUIDs in the metamaterial are close to one of the available stable states of individual SQUIDs. Although the dynamics within each cluster is synchronized, the clusters are not synchronized to each other, resulting in a low degree of synchronization (Fig. 5c). The comparison of Figs. 4c and 5c is very illuminating: the curves obtained for non-locally coupled SQUIDs exhibit a much lower degree of synchronization than the corresponding ones for locally coupled SQUIDs (e.g. for the blue curves, $< |\Psi(\tau)| >_T \simeq 0.42$ and 0.58 for non-local and local coupling, respectively). Moreover, the fluctuations in time are much stronger in the former case, due to the existence of asynchronous cluster(s). For zero initial conditions, both the non-locally and locally coupled SQUID metamaterials give uniform, competely synchronized states with $< |\Psi(\tau)| >_T$ practically equal to unity (not shown). Note that the fluxes in the asynchronous clusters in Figs. 4a and 4b have in general very high amplitude. Similarly to the local coupling case, they correspond to high-flux-amplitude individual SQUID states which cannot be stabilized and therefore they cannot be reached by the SQUIDs in the locally coupled SQUID metamaterial which occupy low-flux-amplitude states (Figs. 5a and 5b). In the non-locally coupled SQUID metamaterial, to the contrary, the additional coupling provided by the second-nearest, third-nearest, etc., neighbors, is capable of keeping the SQUIDs close to these high-flux-amplitude states for long time-intervals.

The spatial profiles of ϕ_n and the time-derivatives of the fluxes averaged over T, $< \dot{\phi}_n(\tau) >_T \equiv < v_n(\tau) >_T$, at the end of the integration time ($\sim 10^7$ t.u.) of Fig. 4a are shown in Figs. 6a and 6b, respectively. Note that $v_n(\tau)$ is the instantaneous voltage across the Josephson junction of the $n-$th rf SQUID. The $< v_n(\tau) >_T$s, corresponding to the time-derivatives of the phases of the oscillators

in Kuramoto-type phase oscillator models, are symmetrically distributed around zero. Notably, the shape of their distribution over the simulation period (not shown) deviates significantly from a Gaussian profile due to correlations between different non-locally interacting clusters. That type of pattern (Fig. 6b) is distinctly different than the standard one for chimera states in phase oscillator models[15], while it resembles the corresponding one for a globally coupled system of complex Ginzburg-Landau oscillators[50]. In Figs. 6a and 6b the synchronous clusters are indicated by horizontal segments; we observe that besides the large incoherent cluster extending from $n = 143$ to 256, there are actually two small ones (at around $n \sim 5$ and $n \sim 112$, more clearly seen in Fig. 6b) which are not visible in Fig. 4a. The calculated value of $< |\Psi| >_T$ as a function of τ for part of the coherent cluster in the blue (small) box of Fig. 6a, that extends from $n = 36$ to 100, is close to unity for all times (blue curve in Fig. 6c). The corresponding curve for the large incoherent cluster in the green (large) box has a significantly lower average value and strong fluctuations which do not decrease with time.

In a real SQUID metamaterial, there is naturally a spread in the parameter values of individual SQUIDs due to fabrication-induced imperfections. The most important source of disorder comes from the critical current of the Josephson junctions, which are very sensitive to the thickness and quality of the insulating layer. As a result, disorder is induced in the SQUID parameters β and their eigenfrequencies Ω_{SQ}. However, with the present technology the spread in β could be less than 1% of its nominal value, which makes the SQUID metamaterial weakly disordered, that could affect the observed chimera states. In order to check the robustness of the chimera states under that perturbation, we performed additional simulations in which β is allowed to vary randomly in an interval up to 5% of its nominal value. For random initial flux configurations, we still obtain chimera states, although with different profiles, due to their high metastability, while for zero initial fluxes we obtain low-amplitude synchronized solutions. We thus conclude that chimera states are robust to weak disorder, and they cannot be generated by weak disorder alone in SQUID metamaterials in the absence of substantial initial fluxes.

The difference in the dynamic behaviour between SQUIDs in the coherent and incoherent clusters is also reflected in the power spectra of $\phi_n(\tau)$. In Fig. 7, two such spectra, one for a SQUID in the coherent cluster ($n = 40$) and one in the incoherent cluster ($n = 190$) of Fig. 4a are shown in logarithmic scale for a range of frequencies around the fundamental (i.e., the driving) one. Note that for the chosen parameters, the resonance frequency $\Omega_{SQ} \simeq \sqrt{1+\beta_L}$, of individual SQUIDs is at $\Omega_{SQ} \simeq 1.3$, while the linear band of the SQUID metamaterial extends from $\Omega_{min} \simeq 1.27$ to $\Omega_{max} \simeq 1.35$ (extracted from the blue curve of Fig. 2). The driving frequency is $\Omega \simeq 1.06$, well below the lower bound of the linear spectrum, Ω_{min}. The spectrum for the SQUID at $n = 40$ (black curve) exhibits very low noise levels and a strong peak at the driving frequency Ω. The smaller peaks in the spectrum of the $n = 40$ SQUID are also part of it, and they are located at frequencies within the linear band of the SQUID metamaterial, i.e., in the range $[\Omega_{min}, \Omega_{max}]$. The longer arrow at right points at the resonance frequency (the eigenfrequency) of individual SQUIDs which is located at $\Omega_{SQ} \simeq 1.3$. Note that only a small number of the eigenfrequencies of the SQUID metamaterial are excited in that spectrum, which seem to be selected by random processes. To the contrary, the spectrum for the SQUID at $n = 190$ exhibits significant fluctuations, the peak at the driving frequency, and in addition a frequency region around $\Omega \sim 0.9 - 1.05$ where the average fluctuation level remains approximatelly constant, forming a shoulder that often appears in such spectra for SQUIDs in an asynchronous cluster of a chimera state.

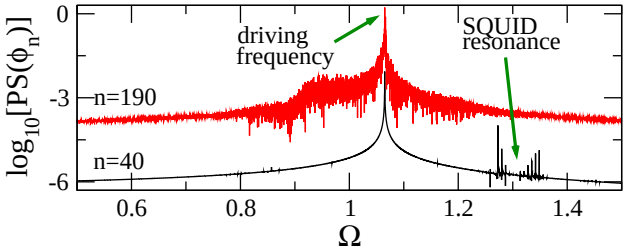

FIG. 7: (Color online) The *power spectra* of $\phi_n(\tau)$ in logarithmic scale for the SQUIDs with $n = 40$ and $n = 190$ that belong to the coherent (black curve) and the incoherent (red curve) cluster, respectively, of Fig. 4a. The arrow at right points at the eigenfrequency of individual SQUIDs, $\Omega_{SQ} \simeq 1.3$.

In order to determine the metastability levels of the states obtained in Figs. 4 and 5, the distributions of $x \equiv < |\Psi(\tau)| >_T$s, $pdf(x)$, at all time-steps over the simulation period were calculated (Fig. 8). A transient period of $100T$ ($\sim$ 5900 t.u.) was allowed, for which the data were discarded. The huge difference of the dispersion of the $x \equiv < |\Psi(\tau)| >_T$ values around their mean $|\bar{\Psi}|$ between non-locally and locally coupled SQUID metamaterial shown in Figs. 8a and 8b, respectively, is readily observed. Consider first the black-solid curves in these figures, which are actually not symmetric but they could fit satisfactorily by an empirical skewed Gaussian function of the form[53,54]

$$pdf(x) = pdf_m \exp\left\{ -\ln(2) \left[\frac{1}{b} \ln\left(1 + \frac{2b(x - x_m)}{D} \right) \right]^2 \right\}, \tag{12}$$

where $pdf_m = pdf(x_m)$ is the maximum of the distribution, x_m is the value of x at which the maximum of the distribution occurs, b is the asymmetry parameter, and D is related to the full-width half-maximum (FWHM) of the distribution, W, by

$$W = D \frac{\sinh(b)}{b}. \tag{13}$$

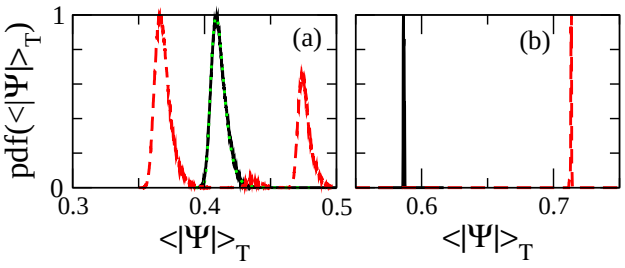

FIG. 8: (Color online) The distributions (divided by their maximum value) of $< |\Psi(\tau)| >_T$s at all instants of the simulation period ($\sim 10^7$ time units with time-step $\Delta t = 0.02$) for the states shown in Figs. 4 and 5. (a) for the chimera states of the non-locally coupled SQUID metamaterial shown in Fig. 4a (black-solid curve) and Fig. 4b (red-dashed curve). The green-dotted curve is a fit with Eq. (12). (b) for the non-uniform states of the locally coupled SQUID metamaterial shown in Fig. 5a (black-solid curve) and Fig. 5b (red-dashed curve).

The green-dotted curve in Fig. 8a is a fit of the black-solid distribution with $b = 0.37$ and $D = 0.0116$, while pdf_m and x_m are taken from the calculated distribution. That fit, and the corresponding one for the black-solid curve in Fig. 8b give, respectively, $W_{nl} \simeq 0.012$ and $W_{loc} \simeq 0.0008$ for the non-locally and locally coupled SQUID metamaterial. For the quantification of the metastability level, we use here the FWHM of the distributions, which for a symmetric Gaussian is directly proportional to the standard deviation $\sigma_{|\Psi|}$. Similarly, the squares of W_{nl} and W_{loc} are proportional to the variance $\sigma^2_{|\Psi|}$ which is a measure of the metastability level. The squares of the calculated FWHMs, W_{nl} and W_{loc}, differ by more than two orders of magnitude, i.e., $(W_{nl}/W_{loc})^2 \simeq 225$, indicating the high metastability level of the chimera state compared to that of the corresponding non-uniform state. Note that for uniform states, that result for zero initial conditions both for non-locally and locally coupled SQUID metamaterials, the FWHM is pactically zero. In Fig. 4b, the high metastability level results in breaking the quasi-stationarity of the chimera state that lasts for $\sim 0.35 \times 10^7$ t.u. through sudden expansions of the upper asynchronous cluster. In that case, the corresponding distribution looks like a "multimodal" one with three peaks (red curve of Fig. 8a); each of them may be however fitted to a skewed Gaussian of the form of Eq. (12). The FWHM for each peak is roughly two order of magnitudes larger than that of the distribution of the corresponding non-uniform state (red curve in Fig. 8b).

IV. CONCLUSIONS

Chimera states are surprising spatiotemporal patterns in which regions of coherence and incoherence coexist. While they were initially discovered in numerical simulations, they have been subsequently observed in several experiments. Notably, these experiments do not merely confirm the numerical and theoretical predictions, but they also reveal other types of interesting collective dynamic behaviour. SQUID metamaterials, which comprise non-locally coupled, nonlinear resonant elements, are physical systems where chimeras or other collective effects could be in principle detected. The emergence of long-lived chimera states in SQUID metamaterials could be acheived by randomly initializing the fluxes threading the SQUID rings. Random initial flux configurations could be achieved by thermal quenching, i.e., by cooling down the SQUID metamaterial through its superconducting transition temperature. As it has been demonstrated in superconducting loops[55] and superconducting thin-film rings[56], spontaneous fluxoid formation may occur through the Kibble-Zurek scenario or by thermal activation, respectively. The Kibble-Zurek scenario has been also confirmed in a multi-Josephson junction superconducting loop[57]. In SQUIDs, however, fluxoid conservation is only approximate, and practically non-existent in non-hysteretic SQUIDs that are considered here. Thus, we would expect that thermal quenching of the SQUID metamaterial could result in a random initial flux configuration, in which the fluxes can take any value (i.e., not only integer multiples of the flux quantum). Note that the random flux configuration is just one possible choice of initial conditions for which chimera states could be observed in SQUID metamaterials.

Our numerical simulations rely on a realistic model, which is capable of reproducing experimental findings such as the tuneability patterns of two-dimensional SQUID metamaterials which are obtained by varying an applied dc flux[5,58]. These simulations indicate that in many cases the coherent and incoherent clusters that make a chimera state maintain their individual sizes for very long times ($> 10^7$ t.u.). During the integration, induced instabilities may lead to sudden expansion of the incoherent cluster(s), or to the desynchronization of narrow coherent clusters. The inherent metastability of the chimera states presented here for the non-locally coupled SQUID metamaterials can be quantified by the strength of the fluctuations of $< |\Psi(\tau)| >_T$. The corresponding locally coupled SQUID metamaterials, in which the interaction between SQUIDs is limited to their first neighbors, supports non-uniform solutions which however are not chimeras. Although both types of states may exhibit a low degree of synchronization, monitored as a function of τ by $< |\Psi(\tau)| >_T$, the fluctuations of the latter in time are much stronger for chimera states than for non-uniform states (more than two orders of magnitude, for the cases shown). Due to their high metastability levels, chimera states are very sensitive to even slight parameter variations. SQUID metamaterials, both in one and two dimensions, have been already fabricated, and some of their dynamical properties have been investigated[2]. Thus, chimera states could in principle be detected with the presently available experimental set-ups.

Acknowledgements

This work was partially supported by the European Union Seventh Framework Programme (FP7-REGPOT-2012-2013-1) under grant agreement n^o 316165, and by the Thales Project MACOMSYS, cofinanced by the European Union (European Social Fund ESF) and Greek national funds through the Operational Program "Education and Lifelong Learning" of the National Strategic Reference Framework (NSRF) Research Funding Program: THALES Investing in Knowledge Society via the European Social Fund. NL and GPT thank Prof. Steven Anlage for illuminating discussions.

[1] S. M. Anlage, J. Opt. **13**, 024001 (2011).
[2] P. Jung, A. V. Ustinov, and S. M. Anlage, Supercond. Sci. Technol. **27**, 073001 (2014).
[3] P. Jung, S. Butz, S. V. Shitov, and A. V. Ustinov, Appl. Phys. Lett. **102**, 062601 (2013).
[4] S. Butz, P. Jung, L. V. Filippenko, V. P. Koshelets, and A. V. Ustinov, Opt. Express **29**, 22540 (2013).
[5] M. Trepanier, D. Zhang, O. Mukhanov, and S. M. Anlage, Phys. Rev. X **3**, 041029 (2013).
[6] P. Jung, S. Butz, M. Marthaler, M. V. Fistul, J. Leppäkangas, V. P. Koshelets, and A. V. Ustinov, Nat. Comms. **5**, 3730 (2014).
[7] B. Josephson, Phys. Lett. A **1**, 251 (1962).
[8] C. Du, H. Chen, and S. Li, Phys. Rev. B **74**, 113105 (2006).
[9] N. Lazarides and G. P. Tsironis, Appl. Phys. Lett. **16**, 163501 (2007).
[10] S. H. Strogatz, Nature **410**, 268 (2001).
[11] S. H. Strogatz, Physica D **143**, 1 (2000).
[12] J. A. Acebrón, L. L. Bonilla, C. J. P. Vicente, F. Ritort, and R. Spigler, Rev. Mod. Phys. **77**, 135 (2005).
[13] D. Battogtokh, Prog. Theor. Phys. **102**, 947 (1999).
[14] R. L. Viana, F. A. dos S. Silva, and S. R. Lopes, Phys. Rev. E **83**, 046220 (2011).
[15] Y. Kuramoto and D. Battogtokh, Nonlinear Phenom. Complex Syst. **5**, 380 (2002).
[16] D. M. Abrams and S. H. Strogatz, Phys. Rev. Lett. **93**, 174102 (2004).
[17] Y. Kuramoto, S.-I. Shima, D. Battogtokh, and Y. Shiogai, Prog. Theor. Phys., Suppl. **161**, 127 (2006).
[18] O. E. Omel'chenko, Y. L. Maistrenko, and P. A. Tass, Phys. Rev. Lett. **100**, 044105 (2008).
[19] D. M. Abrams, R. Mirollo, S. H. Strogatz, and D. A. Wiley, Phys. Rev. Lett. **101**, 084103 (2008).
[20] A. Pikovsky and M. Rosenblum, Phys. Rev. Lett. **101**, 264103 (2008).
[21] E. Ott and T. M. Antonsen, Chaos **19**, 023117 (2009).
[22] E. A. Martens, C. R. Laing, and S. H. Strogatz, Phys. Rev. Lett. **104**, 044101 (2010).
[23] I. Omelchenko, Y. Maistrenko, P. Hövel, and E. Schöll, Phys. Rev. Lett. **106**, 234102 (2011).
[24] N. Yao, Z.-G. Huang, Y.-C. Lai, and Z.-G. Zheng, Sci. Rep. **3**, 3522 (2013).
[25] I. Omelchenko, O. E. Omel'chenko, P. Hövel, and E. Schöll, Phys. Rev. Lett. **110**, 224101 (2013).
[26] J. Hizanidis, V. Kanas, A. Bezerianos, and T. Bountis, Int. J. Bifurcation Chaos **24** , 1450030 (2014).
[27] A. Zakharova, M. Kapeller, and E. Schöll, Phys. Rev. Lett. **112**, 154101 (2014).
[28] T. Bountis, V. Kanas, J. Hizanidis, and A. Bezerianos, Eur. Phys. J.-Spec. Top. **223**, 721 (2014).
[29] A. Yeldesbay, A. Pikovsky, and M. Rosenblum, Phys. Rev. Lett. **112**, 144103 (2014).
[30] M. R. Tinsley, S. Nkomo, and K. Showalter, Nature Phys. **8**, 662 (2012).
[31] A. M. Hagerstrom, T. E. Murphy, R. Roy, P. Hövel, I. Omelchenko, and E. Schöll, Nature Phys. **8**, 658 (2012).
[32] M. Wickramasinghe and I. Z. Kiss, PLOS ONE **8**, e80586 [12 pages] (2013).
[33] S. Nkomo, M. R. Tinsley, and K. Showalter, Phys. Rev. Lett. **110**, 244102 (2013).
[34] E. A. Martens, S. Thutupalli, A. Fourriére, and O. Hallatschek, Proc. Natl. Acad. Sci. **110**, 10563 (2013).
[35] K. Schönleber, C. Zensen, A. Heinrich, and K. Krischer, New J. Phys. **16**, 063024 (2014).
[36] E. A. Viktorov, T. Habruseva, S. P. Hegarty, G. Huyet, and B. Kelleher, Phys. Rev. Lett. **112**, 224101 (2014).
[37] D. P. Rosin, D. Rontani, N. D. Haynes, E. Schüll, and D. J. Gauthier, arXiv: **1405.1950** (2014).
[38] L. Schmidt, K. Schönleber, K. Krischer, and V. García-Morales, Chaos **24**, 013102 (2014).
[39] L. V. Gambuzza, A. Buscarino, S. Chessari, L. Fortuna, R. Meucci, and M. Frasca, Phys. Rev. E **90**, 032905 (2014).
[40] T. Kapitaniak, P. Kuzma, J. Wojewoda, K. Czolczynski, and Y. Maistrenko, Sci. Rep. **4**, 6379 (2014).
[41] A. G. Smart, Physics Today **65**, 17 (2012).
[42] M. J. Panaggio and D. M. Abrams, arXiv: **1403.6204**
[43] N. Lazarides, G. P. Tsironis, and M. Eleftheriou, Nonlinear Phenom. Complex Syst. **11**, 250 (2008).
[44] N. Lazarides and G. P. Tsironis, Proc. SPIE **8423**, 84231K (2012).
[45] N. Lazarides and G. P. Tsironis, Supercond. Sci. Technol. **26**, 084006 (2013).
[46] M. Shanahan, Chaos **20**, 013108 (2010).
[47] M. Wildie and M. Shanahan, Chaos **22**, 043131 (2012).
[48] M. Wolfrum and O. E. Omel'chenko, Phys. Rev. E **84**, 015201 (2011).
[49] R. Singh, S. Dasgupta, and S. Sinha, Europhys. Lett. **95**, 10004 (2011).
[50] G. C. Sethia and A. Sen, Phys. Rev. Lett. **112**, 144101 (2014).
[51] A. Campa, T. Dauxois, and S. Ruffo, Phys. Rep. **480**, 57 (2009).
[52] K. K. Likharev., *Dynamics of Josephson Junctions and Circuits.* (Gordon and Breach, Philadelphia, 1986).
[53] R. D. B. Fraser and E. Suzuki, Anal. Chem. **41**, 37 (1969).
[54] P. F. Rusch and J. P. Lelieur, Anal. Chem. **45**, 1541 (1973).
[55] R. Monaco, J. Mygind, R. J. Rivers, and V. P. Koshelets, Phys. Rev. B **80**, 180501(R) (2009).
[56] J. R. Kirtley, C. C. Tsuei, and F. Tafuri, Phys. Rev. Lett. **90**, 257001 (2003).
[57] R. Carmi, E. Polturak, and G. Koren, Phys. Rev. Lett. **84**, 4966 (2000).
[58] G. P. Tsironis, N. Lazarides, and I. Margaris, Appl. Phys. A **117**, 579 (2014).